Ionics (2020) 26:5385–5392
https://doi.org/10.1007/s11581-020-03726-y

ORIGINAL PAPER

Dendritic micro-nano $NiCo_2O_4$ anode material generated from chemical dealloying for high-performance lithium-ion batteries

Man Zhang[1,2] · Dongwei Li[1] · Lijie Yang[3] · Huan Shi[1] · Yuxia Liu[2]

Received: 19 April 2020 / Revised: 29 July 2020 / Accepted: 30 July 2020 / Published online: 10 August 2020

Abstract

CoNi-contained nanosheets can be prepared by dealloying CoNiAl alloys in aqueous NaOH solution in the presence of H_2O_2, and upon annealing sample exhibits dendritic $NiCo_2O_4$ micro-nanostructure. The effect of H_2O_2 solution on the structure, morphology, and electrochemical performances of the resulting products is studied systematically. These results indicate that the H_2O_2 solution mainly influences the morphology of the $NiCo_2O_4$. When tested as anode materials for lithium-ion batteries (LIBs), the obtained $NiCo_2O_4$ sample shows high specific capacity, excellent rate property, and superb cycling stability. A reversible capacity is still maintained at 1016.9 mAh/g after 100 cycles at a current density of 100 mA/g. Even at a current rate of 1000 mA/g, the capacity can reach to 691.4 mAh/g. The outstanding electrochemical properties of the $NiCo_2O_4$ anode make them promising anode materials of LIBs and other energy storage applications.

Keywords Dealloying · Lithium-ion battery · Anode materials · Dendritic structure · $NiCo_2O_4$

Introduction

Lithium-ion batteries (LIBs) as one of the most promising rechargeable energy storage devices are widely applied in electric vehicles (EVs) and hybrid electric vehicles (HEVs) [1–3]. The anode material often plays an important role in the determination of the energy density, safety, and cycling life of LIBs. Graphite has been widely used as the commercialized anode due to its excellent cycling stability and relatively small volume change of only 12% during lithiation/delithiation [4, 5]. However, this material offers low theoretical capacity (LiC_6, 372 mAh/g) and low delithiation potential (0.05 V vs. Li^+/Li) [6, 7]. Obviously, it is an unsuitable anode material for the next-generation LIBs required for smart electrical grid systems and wearable electronic devices. It is required to construct novel anode materials of higher Li-storage capability and operational safety than graphite. The primary candidates are transition metal oxides (TMOs) due to special lithium oxidation reduction storage mechanism in a reversible manner, resulting in high theoretical capacities [8].

Among the various TMOs, bimetallic oxide, with synergetic enhanced activities by modifying two components with each other, usually gains better performance. $NiCo_2O_4$ as one of bimetallic oxides with high theoretical specific capacity (891 mAh/g) is considered as a promising electrode material [1]. Moreover, $NiCo_2O_4$ possesses higher electronic conductivity compared with NiO or Co_3O_4, which is beneficial for the electron transfer during cycling [9]. In addition, the Co and Ni elements are low-toxicity during melting process, low cost and abundant in the earth, which improves the attraction of $NiCo_2O_4$. Nevertheless, during the charging/discharging process, the sluggish reaction kinetics and drastic volume change lead to poor rate performance and short cycling life, restricting

Electronic supplementary material The online version of this article (https://doi.org/10.1007/s11581-020-03726-y) contains supplementary material, which is available to authorized users.

✉ Dongwei Li
dwli@sdas.org

✉ Yuxia Liu
liuyuxia2008@163.com

[1] Advanced Materials Institute, Qilu University of Technology (Shandong Academy of Sciences), Jinan 250014, China

[2] The Key Laboratory of Life-Organic Analysis, Key Laboratory of Pharmaceutical Intermediates and Analysis of Natural Medicine, School of Chemistry and Chemical Engineering, Qufu Normal University, Qufu 273165, Shandong, China

[3] College of Basic Medicine, Jining Medical University, Jining 272067, China

its commercial application in LIBs. Numerous efforts have been made to tackle this issue. One is to construct nanostructured $NiCo_2O_4$ to reduce the diffusion distance of Li ion during charging/discharging process and thus alleviate the volume expansion/shrinkage [10–12]. For example, Anchali Jain et al. synthesized porous $NiCo_2O_4$ nanodisks through facile and straightforward hydrothermal process. The electrode delivered a discharge capacity of 673.9 mAh/g after 350 cycles at the current density of 0.5 C [13]. Jin et al. fabricated hydrangea-like $NiCo_2O_4$ through a solvothermal method. At a current density of 100 mA/g, the discharge specific capacity was up to 928 mAh/g after 100 cycles [14]. Although many methods have been developed to fabricate nanostructural $NiCo_2O_4$ anode materials with good Li ion storage properties, a simpler and proper synthetic route to a mass production of $NiCo_2O_4$ with high performance is still need to be explored.

Dealloying has been recognized to be an effective strategy for the fabrication of functional TMOs via selective dissolution of one or more active elements out of suitable precursor alloys [15, 16]. Ding prepared hierarchically porous MnO_x microspheres by dealloying method followed by mediate temperature annealing. The porous MnO_x microspheres showed a promising electrochemical performance as an advanced anode material in LIBs with a specific capacity of 757 mAh/g at 500 mA/g after 100 cycles [17]. Liu et al. designed porous $CoFe_2O_4$ nanoplates through dealloying Co4Fe8Al88 precursor ribbons. The as-obtained $CoFe_2O_4$ nanoplates exhibited high capacity, long cycle life, and good rate capability as an anode material for LIBs [18]. In present work, we provide a modified dealloying process to the fabrication of dendritic micro-nanostructural $NiCo_2O_4$ anode material. The different concentrations of H_2O_2 solution are controlled during the dealloying process, and two typical nanostructured products are obtained by this melt spinning and dealloying method. The electrochemical performances of these nanocomposites are investigated in details. The dendritic micro-nano $NiCo_2O_4$ electrode with high surface area shows high specific capacity and superior cycling reversibility, showing the encouraging application potential as an advanced anode material for LIBs.

Experimental method

The synthesis procedure of $NiCo_2O_4$ is schematically illustrated in Fig. 1 (see the supporting information for experimental details). Al-based CoNiAl alloy is chosen as the precursor alloy due to the more reactive property and low cost of Al. $NiCo_2O_4$ prepared by dealloying in sodium hydroxide is recorded as $NiCo_2O_4$-NaOH, while in the mixture solution of sodium hydroxide and hydrogen peroxide is marked as $NiCo_2O_4$-NaOH+H_2O_2. The annealed bimetallic oxides are recorded as $NiCo_2O_4$-NaOH-500 and $NiCo_2O_4$-NaOH+H_2O_2-500, respectively.

Results and discussion

Structural and morphologies

Thermogravimetric analysis (TGA) is carried out from room temperature to 600 °C with temperature gradient of 10 °C/min in air. Figure 2 shows the typical TGA curves of $NiCo_2O_4$-NaOH+H_2O_2-500, which can be used to demarcate the actual content of each component and investigate the thermal stability of $NiCo_2O_4$. The physically combined water molecules are the first to leave below 100 °C. The gradual weight loss of about 24.5% can be attributed to oxidation of the Ni/Co hydroxide as the temperature is increased to 500 °C and the remaining component is $NiCoO_x$ [19]. After 500 °C, no obvious decline in quality is observed, indicating that $NiCoO_x$ is relatively stable in composites.

To confirm the phase structure of $NiCoO_x$ composites, X-ray diffraction (XRD) is conducted, as shown in Fig. 3a. It is obvious that the major diffraction peaks agree with the standard reference pattern of $NiCo_2O_4$ (PDF# 73-1702). This result indicates that the utilized dealloying condition is favorable for the formation of pure $NiCo_2O_4$. XPS spectra are acquired to analyze the electronic structures of $NiCo_2O_4$. Figure 3b shows the Ni 2p XPS spectrum. The spectrum can be deconvoluted into four peaks, including Ni $2p_{3/2}$ (853.8 eV), Ni $2p_{1/2}$ (873.1 eV) and two satellite peaks [20]. An XPS high-resolution scan of the Co 2p core level is shown in Fig. 3c. The Co $2p_{3/2}$ peak and Co $2p_{1/2}$ peak are centered at 779.9 eV and 794.8 eV, being consistent with the bivalent oxidation state of Co. The peaks at 783.9 eV and 804.1 eV are corresponding shakeup satellites of Co $2p_{3/2}$ peak and Co $2p_{1/2}$ peak, respectively, which further confirmed that Co mainly exists in the Co^{2+} and Co^{3+} state [21]. Furthermore, the O 1 s core level spectra (Fig. 3d) can be resolved into three peaks, centered at 530.2, 531.8, and 533.0 eV, respectively. The low-binding-energy peak observed at 530.2 eV is attributed to OM oxygen, corresponding to O^{2-} ions in transition metal oxide. The latter two peaks are assigned to OH and OH_2, respectively [22]. The XPS results indicate that the metal elements in the $NiCo_2O_4$ composites exist in the form of Ni^{2+}, Ni^{3+}, Co^{2+}, and Co^{3+}, which are in good agreement with results of $NiCo_2O_4$ in the literature.

We have investigated the effect of H_2O_2 and annealing on the controllable morphology. The morphology and microstructure of as-prepared samples are investigated by SEM and TEM. Figure 4a and b show that the $NiCo_2O_4$-NaOH precursors are mainly irregular nanosheet with thickness of ~ 30 nm. As shown in Fig. 4c and d, in the present of H_2O_2, thinner nanosheets will form, which will eventually evolve into more

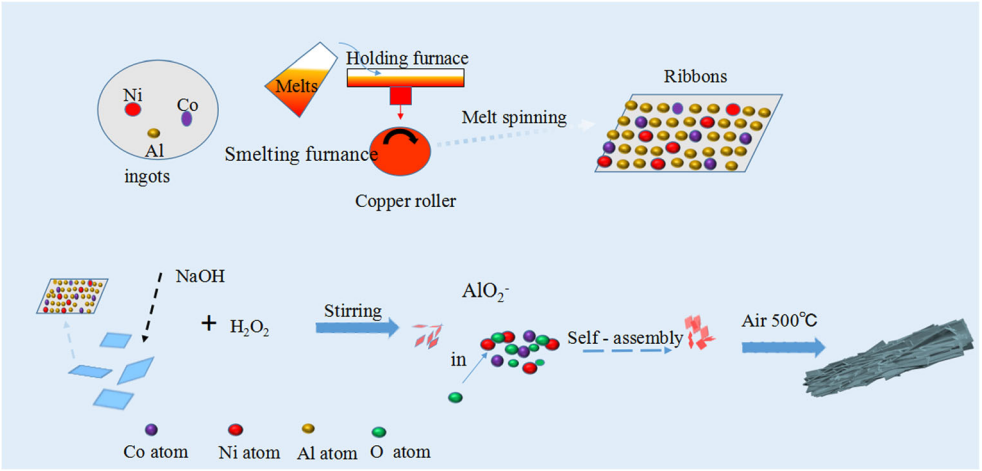

Fig. 1 Schematic illustration of the formation process of $NiCo_2O_4$

uniform aggregates suggesting the role of H_2O_2 to provide centers of heterogeneous nucleation during processing [23]. After thermal decomposition at 500 °C, these nanosheets transform into dendritic structure along with the thin nanosheets turning into nanorods (Fig. 4e, f), forming a unique hierarchitecture with two degrees of structural characteristics at both nanometer and micrometer scales. Apparently, such in-site growth of dendritic structure not only improves the structural integrity but also effectively reduces the contact resistance among nanorods. TEM image provides the detailed microstructure of the obtained $NiCo_2O_4$-NaOH+H_2O_2-500 sample. As displayed in Fig. 4g, the sample consists of a large number of closely packed nanoflakes with a length of ~ 30–40 nm and a thickness of ~ 2–3 nm, which is in accordance with that from SEM observation. HRTEM image (Fig. 4h) provides more detail, in which the clear lattice fringes can be easily observed, with the spacing calculated to be ~ 0.25 nm, which can be ascribed to the (311) planes of $NiCo_2O_4$. Through the comparison of Fig. 4a–h, it is found that a multistage dendritic rod-shaped micro-nanostructure assembled from nanosheets can be controllably prepared by a modified dealloying method followed by mediate temperature annealing. A novel idea of designing micro-nanostructure is presented.

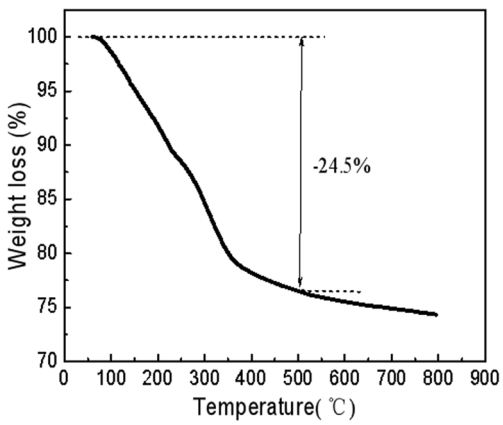

Fig. 2 TGA curve of the $NiCo_2O_4$-NaOH+H_2O_2-500

Figure 5a–d show the element mapping analysis of $NiCo_2O_4$-NaOH+H_2O_2-500. The distribution of Co, Ni, O, and Al are relatively uniform in the dendritic micro-nanostructure. As depicted in Fig. 5e, the elements in the selected region are Co, Ni, O, and Al, and most abundant O element is observed, which reconfirms that the main component is in the presence of $NiCo_2O_4$ [24–26]. The atom ratio of Ni and Co is approximately 1:2, which is close to that in the precursor ribbons [27]. According to the dealloying mechanism, the residual Al (several atom percent) is detectable in the as-dealloyed sample [28]. The results of element mapping and energy spectrum analysis indicate that $NiCo_2O_4$ material exists in oxidation state and the distribution of Co, Ni, and O elements is relatively uniform.

Electrochemical performance

Electrochemical tests including cyclic voltammetry (CV) and galvanostatic discharge-charge (GDC) cycling were conducted to evaluate the performance of the $NiCo_2O_4$ electrode. Figure 6a shows the CV curves of the first three cycles in the voltage range of 0.01–3.0 V (vs. Li^+/Li) at a scan rate of 0.1 mV/s. In the first discharge process, the main peaks at 0.3 V and 0.75 V could be attributed to the reduction of Ni^{2+}, Ni^{3+}, Co^{2+}, and Co^{3+} to their metallic states, respectively [19]. The small broad peak located at 0.10 V refers to the formation of a solid/electrolyte interface (SEI) generated from the decomposition of electrolyte. The electrochemical reaction of discharge can be shown as:

$$NiCo_2O_4 + 8Li^+ + 8e^- \rightarrow Ni + 2Co + 4Li_2O$$

In the following cycles, the peaks shift to 0.85 V and 1.5 V. The obvious difference between the peaks in the first and subsequent cycles is mainly due to the irreversible capacity loss of

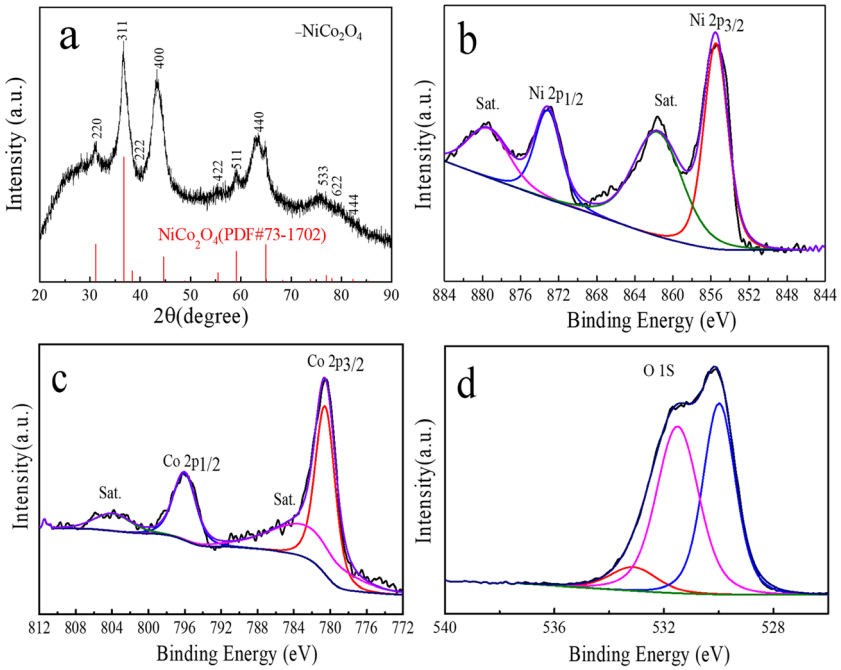

Fig. 3 (**a**) XRD patterns of the dealloyed $NiCo_2O_4$-NaOH+H_2O_2-500 with reference to the standard spectrum card. XPS spectra of the $NiCo_2O_4$: (**b**) Ni 2p, (**c**) Co 2p, (**d**) O 1 s

the anode materials observed during the first cycle, as well as the polarization of the electrode material [29, 30]. In the charge process, there are three oxidation peaks at 0.47 V, 1.4 V, and 2.3 V, which probably related to the multistep oxidation of metallic Ni and Co to their oxide states, together with the decomposition of SEI film and Li_2O [31, 32]. After the first cycle, the redox peaks almost remain consistent, indicating relatively good reversibility of the $NiCo_2O_4$ nanocomposites.

The initial three discharge/charge cycles of $NiCo_2O_4$ nanocomposites at 100 mA/g are displayed in Fig. 6b. During the first discharge process, it exhibits a conspicuous voltage plateaus between 1.0 and 0.6 V and a total capacity of ~ 868.5 mAh/g, while it delivers an initial charge capacity of 522.7 mAh/g. The irreversible capacity of the first cycle is attributed to the formation of SEI [33]. There are obvious charging platforms at 0.3–0.47 V, 0.47–1.4 V, and 1.4–2.3 V, attributing to the oxidation of Ni and Co and the decomposition of SEI [34, 35]. In the subsequent cycle, the discharge voltage platform shifts to 1.5 V. Four obvious discharge platforms are observed (between 3 and 1.5 V, 1.5–0.85 V, 0.85–0.3 V, and 0.3–0.2 V), which agrees with the CV results. The discharge/charge profiles almost overlap after the first cycle, indicating an excellent stability after the initial.

To better understand the electrochemical performance of the new electrode, we compared the cycling performance of $NiCo_2O_4$-NaOH, $NiCo_2O_4$-NaOH-500, $NiCo_2O_4$-NaOH+H_2O_2, and $NiCo_2O_4$-NaOH+H_2O_2-500 electrodes at the same current density, as shown in Fig. 6c. It is noteworthy that the $NiCo_2O_4$-NaOH+H_2O_2 electrode shows higher capacities than $NiCo_2O_4$-NaOH and $NiCo_2O_4$-NaOH-500 before 30 cycles, followed by a quick fall in capacity in prolonged cycles. The capacities of the uncalcined electrode all fade quickly after several cycles. Remarkably, the $NiCo_2O_4$-NaOH+H_2O_2-500 electrode exhibits excellent cyclic stability. These capacities of 1537.4 mAh/g and 1117.4 mAh/g are obtained at first and second cycle. Reversible capacity as high as 1019.6 mAh/g after 100 cycles can still be obtained at a current density of 100 mA/g, which is higher than the theoretical capacity. The SEM image indicates that the samples without H_2O_2 are mainly irregular nanosheets, while the samples with H_2O_2 have good crystallinity and exist as dendritic rod-shaped structures. After thermal decomposition at 500 °C, these nanosheet materials transform into micro-nanostructure, forming a unique hierarchitecture with two degrees of structural characteristics at both nanometer and micrometer scales. The improved cycling stability should be attributed to the micro-nanostructure assembled by dendritic rod, which can not only buffer the huge volume change of active material during discharge/charge process but also enhance the lithium-ion diffusion and electron transport [36, 37]. Table S1 compares the key electrochemical performance parameters of $NiCo_2O_4$ and the relevant TMOs between literature results and present work. The optimized $NiCo_2O_4$-NaOH+H_2O_2-500 nanocomposites have excellent cycling stability.

To better understand the superior cycling performance of $NiCo_2O_4$-NaOH+H_2O_2-500 electrode, the morphology after 100 discharge/charge cycles at 100 mA/g is investigated as presented in Fig. S1. The surface becomes rough, and some areas are clogged upon cycling. Nevertheless, the overall dendritic morphology is basically retained, indicating a good structure stability of $NiCo_2O_4$-NaOH+H_2O_2-500.

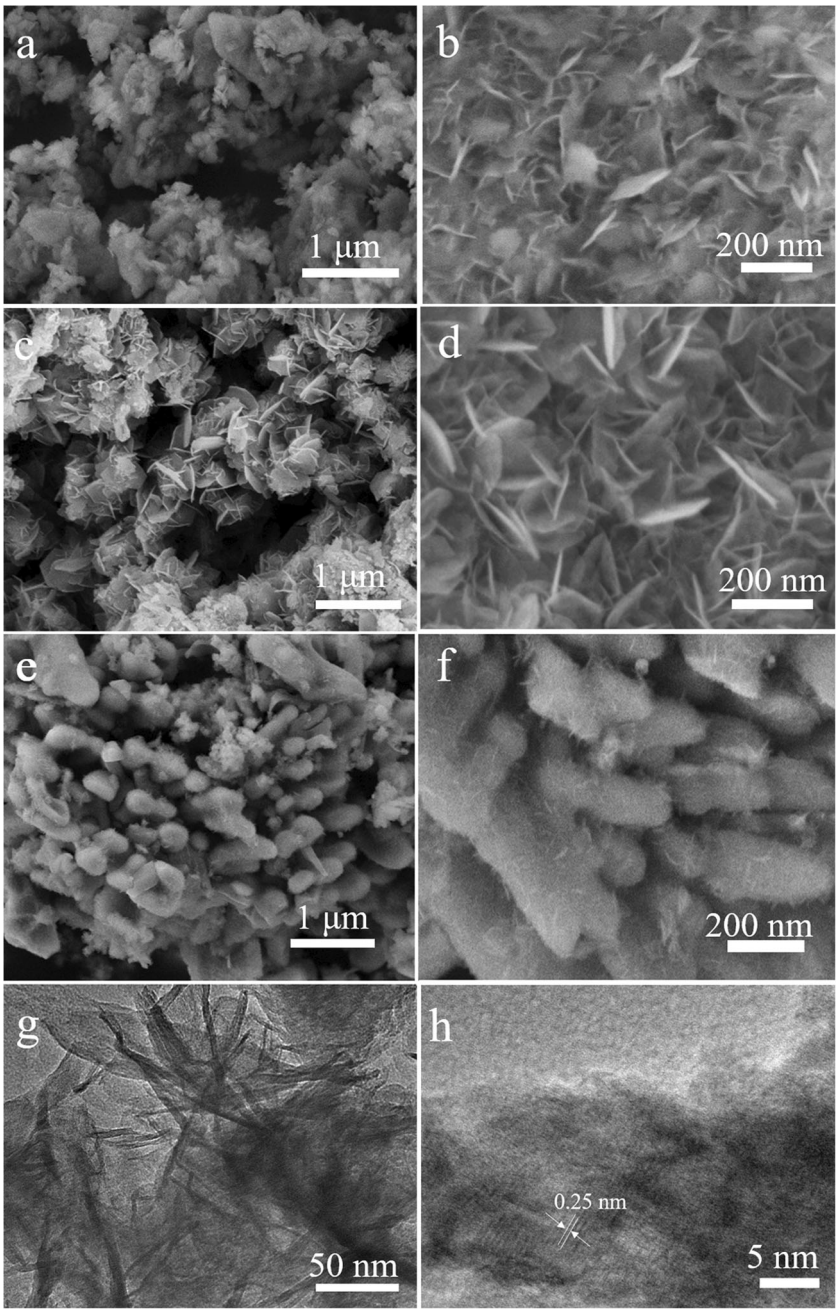

Fig. 4 SEM images of the $NiCo_2O_4$ electrodes: (**a**–**b**) $NiCo_2O_4$-NaOH, (**c**–**d**) $NiCo_2O_4$-NaOH+H_2O_2, (**e**–**f**) $NiCo_2O_4$-NaOH+H_2O_2-500. (**g**) TEM image and (**h**) HRTEM image of $NiCo_2O_4$-NaOH+H_2O_2-500

Dealloying time is an important parameter, and thus we investigate the electrochemical behaviors of $NiCo_2O_4$-NaOH+H_2O_2-500 materials obtained with controlled dealloying times (24 h, 48 h, and 64 h). For convenience, the fresh products dealloyed by different time are labeled as D-24 h, D-48 h, and D-64 h, respectively. Figure 7a depicts the cycling performance at the current density of 100 mA/g, both of which show a similar capacity trend. In particular, the D-64 h exhibits excellent cycle stability, retaining reversible specific capacity as high as 1016.9 mAh/g after 100 cycles, whereas comparable discharge capacities of 792.8 and 1009 mAh/g are obtained for D-24 h and D-48 h, respectively.

Apart from the high specific capacity and good cyclability, rate capability is another very important property for high-performance LIBs. Figure 7b–d show the rate performance of D-24 h, D-48 h and D-64 h electrodes at various current densities between 3.0 and 0.01 V. At the current densities of 100, 200, 500, and 1000 mA/g, the D-64 h anode shows the good rate capacity, with an average discharge capacity of 1385.2, 1160.3, 940.4, and 691.4 mAh/g, respectively. Another impressive result is the restoration of the D-64 h after high rate cycling. When the current density restores to 100 mA/g, the cell can recover a high reversible capacity of 1281.5 mAh/g. The reversible capacity of D-48 h is 867,

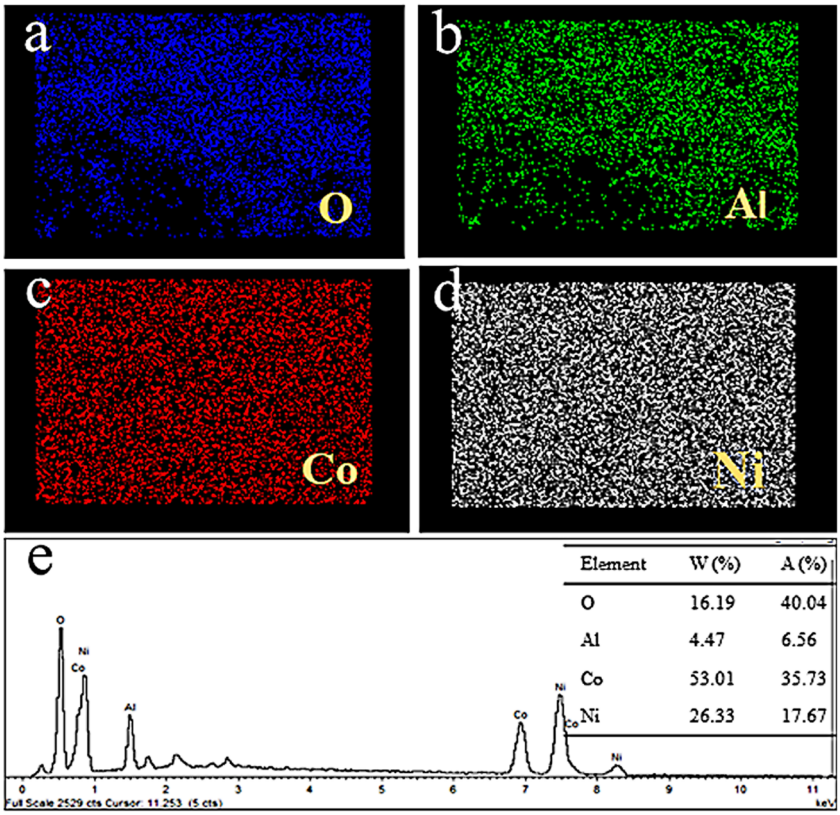

Fig. 5 The element mapping images for (**a**–**d**): O, Al, Co, and Ni, respectively. (**e**) Energy spectrum analysis of $NiCo_2O_4$-NaOH+H_2O_2-500

727.2, 530, 409.8, and 738 mAh/g, respectively, and meanwhile, the D-64 h anode shows the average capacity of 832.2, 695.1, 464, and 259.5 mAh/g, respectively. The results demonstrate that the D-64 h nanocomposites have the good cyclic stability and exceptional rate capability. It can ensure that the material structure will not be damaged in the process of rapid charge and discharge. Therefore, the D-64 h anode can accommodate the large current density changes.

For the direct and further understanding of the electrochemical superiority of the D-64 h electrode, electrochemical impedance spectroscopy (EIS) measurements for the three electrodes are conducted at an open-circuit voltage state using

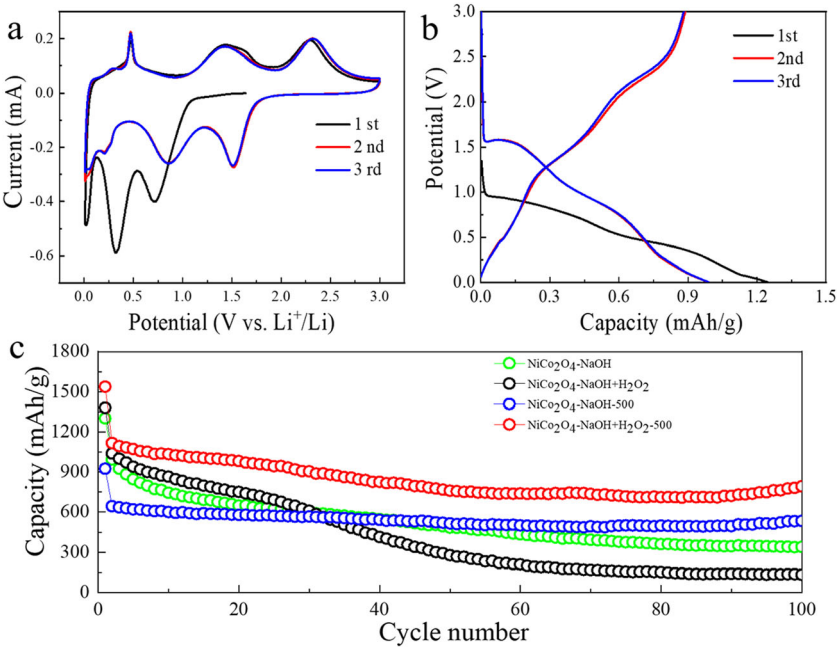

Fig. 6 (**a**) CV curves of the first three cycles for the $NiCo_2O_4$-NaOH+H_2O_2-500 nanocomposites at a scan rate of 0.1 mV/s in the voltage window of 0.01–3.0 V (vs. Li^+/Li). (**b**) Discharge/charge profiles of the three cycles for the $NiCo_2O_4$-NaOH+H_2O_2-500 nanocomposites at a current density of 100 mA/g. (**c**) Cycling performance of $NiCo_2O_4$-NaOH, $NiCo_2O_4$-NaOH-500, $NiCo_2O_4$-NaOH+H_2O_2, and $NiCo_2O_4$-NaOH+H_2O_2-500 at a current density of 100 mA/g

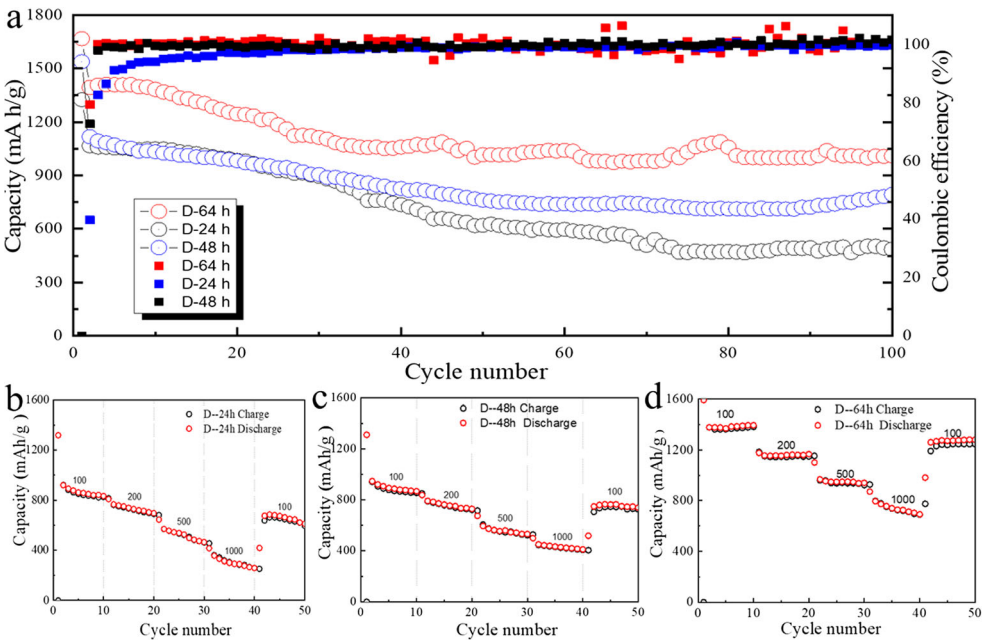

Fig. 7 (**a**) Cycling performance of $NiCo_2O_4$-NaOH+H_2O_2-500 nanocomposites prepared with different dealloying time at 100 mA/g. (**b**) Rate capabilities of $NiCo_2O_4$-NaOH+H_2O_2-500 nanocomposites prepared by dealloying 24 h at a current density of 100 mA/g. (**c**) 48 h. (**d**) 64 h

fresh cells and the resulting Nyquist profiles are presented in Fig. 8. In the high-frequency region, each curve consists of a depressed semicircle, representing the charge-transfer impedance of the cell. Meanwhile, a sloping line in low-frequency region exists in each plot, which is related to the mass transfer of Li ion [38]. It is clearly observed that the big difference focuses on the diameter of the three semicircles, which is proportional to the value of the charge-transfer impedance (R_{ct}). As showed, the D-64 h anode exhibits the lowest R_{ct} value. And the linear Warburg impedance (Z_w) is a slope of approximately 45° in the low-frequency region corresponding to the Li ion diffusion process in the electrodes. These results are in good agreement with the electrochemical performance of D-64 h electrode. The outstanding electrochemical performance should be attributed to its unique structure and multi-components. With this structure, the special dendritic micro-nano structure provides a short diffusion length for Li ion, and offer available space to accommodate the volume changes of

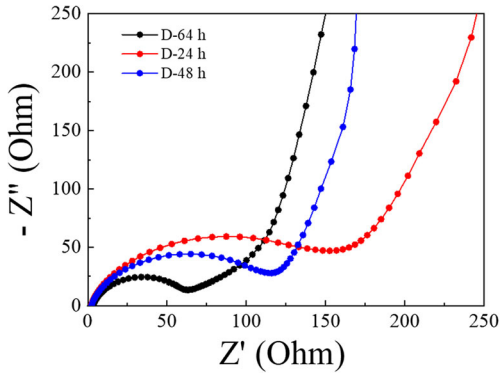

Fig. 8 EIS spectra of the $NiCo_2O_4$-NaOH+H_2O_2-500 nanocomposites prepared with different dealloying time

the during the cycling performance. Meanwhile, the mixed conductive metal Co/Ni in the composite facilitates electron transfer. Therefore, the capacity retention and kinetics are both improved.

Conclusions

In conclusion, dendritic micro-nanostructural $NiCo_2O_4$ materials are successfully synthesized by a simple melt spinning-dealloying method followed by mediate temperature annealing. The D-64 h electrodes deliver superb specific capacity, good rate performance, and outstanding cycling stability. A capacity of 1016.9 mA/g at a current density of 100 mA/g is obtained after 100 cycles. The special structure favors the enhanced electrochemical performance. On the one hand, the large number of nanosheets in $NiCo_2O_4$ significantly increases the contact area between the electrode and the electrolyte, thus shortening the Li-ion transmission path. On the other hand, the uniform distribution of micro-nanostructure is beneficial to reduce the strain caused by volume changes during the long-term discharge/charge cycle, which can greatly improve the cycling capacity. Owing to the superiorities of high lithium storage performances and easy preparation, the dendritic micro-nanostructural $NiCo_2O_4$ shows encouraging application potential as an advanced anode material for LIBs.

Funding information This work was supported by the Natural Science Foundation of Shandong Province (ZR2017BEM020 and ZR2019PB019) and Major Science and Technological Innovation Project of Shandong Province (2019JZZY010457).

Compliance with ethical standards

Conflict of interest The authors declare that they have no conflict of interest.

References

1. Han X et al (2018) Recent progress of $NiCo_2O_4$-based anodes for high-performance lithium-ion batteries. Curr Opinion Solid State Mater Sci 22(4):109–126
2. Fu F et al (2017) Hierarchical $NiCo_2O_4$ micro- and nanostructures with tunable morphologies as anode materials for lithium- and sodium-ion batteries. ACS Appl Mater Interfaces 9(19):16194–16201
3. Qin B et al (2017) Ultrafast ionic liquid-assisted microwave synthesis of SnO microflowers and their superior sodium-ion storage performance. ACS Appl Mater Interfaces 9(32):26797–26804
4. Wang J et al (2014) Structural evolution and pulverization of tin nanoparticles during lithiation-delithiation cycling. J Electrochem Soc 161(11):F3019
5. Kamali AR et al (2011) Tin-based materials as advanced anode materials for lithium ion batteries: a review. Rev Adv Mater Sci 27(1):14–24
6. Liu Q et al (2019) Double conductivity-improved porous Sn/Sn_4P_3@ carbon nanocomposite as high-performance anode in lithium-ion batteries. J Colloid Interface Sci 537:588–596
7. Wetjen M et al (2018) Morphological changes of silicon nanoparticles and the influence of cutoff potentials in silicon-graphite electrodes. J Electrochem Soc 165(7):A1503
8. Zheng M et al (2018) Hierarchically nanostructured transition metal oxides for lithium-ion batteries. Adv Sci (Weinh) 5(3):1700592
9. Yuvaraj S et al (2016) An overview of AB_2O_4-and A_2BO_4-structured negative electrodes for advanced Li-ion batteries. RSC Adv 6(26):21448–21474
10. Zhu Y et al (2015) A simple synthesis of two-dimensional ultrathin nickel cobaltite nanosheets for electrochemical lithium storage. Electrochim Acta 176:141–148
11. Zhou X et al (2015) One-dimensional $NiCo_2O_4$ nanowire arrays grown on nickel foam for high-performance lithium-ion batteries. J Power Sources 299:97–103
12. Zhang C et al (2020) $NiCo_2O_4$/biomass-derived carbon composites as anode for high-performance lithium ion batteries. J Power Sources 451:227761
13. Jain A et al (2019) Two-dimensional porous nanodisks of $NiCo_2O_4$ as anode material for high-performance rechargeable lithium-ion battery. J Alloys Compd 772:72–79
14. Jin R et al (2016) High electrochemical performances of hierarchical hydrangea macrophylla like $NiCo_2O_4$ and $NiCo_2S_4$ as anode materials for Li-ion batteries. Mater Res Bull 80:309–315
15. McCue I et al (2016) Dealloying and dealloyed materials. Annu Rev Mater Res 46:263–286
16. Xu C et al (2010) A general corrosion route to nanostructured metal oxides. Nanoscale 2(6):906–909
17. Jiang X et al (2015) Dealloying to porous hybrid manganese oxides microspheres for high performance anodes in lithium ion batteries. J Power Sources 274:862–868
18. Wang Z et al (2017) $CoFe_2O_4$ nanoplates synthesized by dealloying method as high performance Li-ion battery anodes. Electrochim Acta 252:295–305
19. Rong H et al (2018) A novel $NiCo_2O_4$@GO hybrid composite with core-shell structure as high-performance anodes for lithium-ion batteries. J Alloys Compd 731:1095–1102
20. Marco J et al (2000) Characterization of the nickel cobaltite, $NiCo_2O_4$, prepared by several methods: an XRD, XANES, EXAFS, and XPS study. J Solid State Chem 153(1):74–81
21. Xiong S et al (2009) Controllable synthesis of mesoporous Co_3O_4 nanostructures with tunable morphology for application in supercapacitors. Chem Eur J 15(21):5320–5326
22. Wang J et al (2017) C@$CoFe_2O_4$ fiber-in-tube mesoporous nanostructure: formation mechanism and high electrochemical performance as an anode for lithium-ion batteries. J Alloys Compd 693:110–117
23. Chen Z et al (2012) Recent advances in manganese oxide nanocrystals: fabrication, characterization, and microstructure. Chem Rev 112(7):3833–3855
24. Lu Q et al (2013) Ordered mesoporous nickel cobaltite spinel with ultra-high supercapacitance. J Mater Chem A 1(6):2331–2336
25. Wang Y et al (2010) Excellent performance in lithium-ion battery anodes: rational synthesis of Co $(CO_3)_{0.5}(OH)_{0.11}H_2O$ nanobelt array and its conversion into mesoporous and single-crystal Co_3O_4. ACS Nano 4(3):1425–1432
26. Liu Q et al (2019) Hierarchical mulberry-like Fe_3S_4/Co_9S_8 nanoparticles as highly reversible anode for lithium-ion batteries. Electrochim Acta 304:405–414
27. Chen Z et al (2019) Carbon particles modified macroporous Si/Ni composite as an advanced anode material for lithium ion batteries. Int J Hydrog Energy 44(2):1078–1087
28. Liu B et al (2019) A three-dimensional multilevel nanoporous $NiCoO_2$/Ni hybrid for highly reversible electrochemical energy storage. J Mater Chem A 7(27):16222–16230
29. Sun X et al (2014) Multifunctional Ni/NiO hybrid nanomembranes as anode materials for high-rate Li-ion batteries. Nano Energy 9:168–175
30. Sun X et al (2016) High-defect hydrophilic carbon cuboids anchored with Co/CoO nanoparticles as highly efficient and ultrastable lithium-ion battery anodes. J Mater Chem A 4(26):10166–10173
31. Wei Y et al (2015) Solvent-controlled synthesis of NiO–CoO/carbon fiber nanobrushes with different densities and their excellent properties for lithium ion storage. ACS Appl Mater Interfaces 7(39):21703–21711
32. Sun Y et al (2012) Ultrathin CoO/graphene hybrid nanosheets: a highly stable anode material for lithium-ion batteries. J Phys Chem C 116(39):20794–20799
33. Li J et al (2013) High electrochemical performance of monodisperse $NiCo_2O_4$ mesoporous microspheres as an anode material for Li-ion batteries. ACS Appl Mater Interfaces 5(3):981–988
34. Hu L et al (2012) $CoMn_2O_4$ spinel hierarchical microspheres assembled with porous nanosheets as stable anodes for lithium-ion batteries. Sci Rep 2:986
35. Mondal AK et al (2014) Highly porous $NiCo_2O_4$ nanoflakes and nanobelts as anode materials for lithium-ion batteries with excellent rate capability. ACS Appl Mater Interfaces 6(17):14827–14835
36. Yang Y et al (2018) Preparation and electrochemical properties of mesoporous $NiCo_2O_4$ double-hemisphere used as anode for lithium-ion battery. J Colloid Interface Sci 529:357–365
37. Liu Q et al (2020) TiO_2 particles wrapped onto macroporous germanium skeleton as high performance anode for lithium-ion batteries. Chem Eng J 381:122649
38. Chen Z et al (2019) Graphene quantum dots modified nanoporous SiAl composite as an advanced anode for lithium storage. Electrochim Acta 318:228–235